Eur. Phys. J. B **17**, 269–279 (2000)

**THE EUROPEAN PHYSICAL JOURNAL B**

EDP Sciences


# Damage in fiber bundle models

F. Kun[1,2,a], S. Zapperi[3,4], and H.J. Herrmann[1,3]

[1] ICA 1, University of Stuttgart, Pfaffenwaldring 27, 70569 Stuttgart, Germany
[2] Department of Theoretical Physics, University of Debrecen, PO Box 5, 4010 Debrecen, Hungary
[3] PMMH-ESPCI, 10 rue Vauquelin, 75231 Paris Cedex 05, France
[4] INFM sezione di Roma 1, Università "La Sapienza", P.le A. Moro 2 00185 Roma, Italy

Received 27 March 2000

**Abstract.** We introduce a continuous damage fiber bundle model and compare its behavior with that of dry fiber bundles. Several interesting constitutive behaviors, such as plasticity, are found in this model depending on the value of the damage parameter and on the form of the disorder distribution. We compare the constitutive behavior of global load transfer models, obtained analytically, with local load transfer models numerical simulations. The evolution of the damage is studied analyzing the cluster statistics for dry and continous damage fiber bundles. Finally, it is shown that quenched random thresholds enhance damage localization.

**PACS.** 46.50.+a Fracture mechanics, fatigue and cracks – 62.20.Fe Deformation and plasticity (including yield, ductility, and superplasticity) – 62.20.Mk Fatigue, brittleness, fracture, and cracks

## 1 Introduction

The rupture of disordered media has recently attracted much technological and industrial interest and has been widely studied in statistical physics. It has been suggested by several authors that the failure of a disordered material subjected to an increasing external load shares many features with thermodynamic phase transitions. In particular, a stressed solid can be considered to be in a metastable state [1] and the point of global failure can be seen as a nucleation process in a first order transition near a spinodal [2–4]. Thus, the power law behavior observed experimentally in the acoustic emission before failure [5–7] has been compared with the mean-field scaling expected close to a spinodal point [8]. In analogy with spinodal nucleation [9], scaling behavior can only be seen when long-range interactions are present, as it is the case for elasticity, but should not be observable when the stress transfer function is short ranged. This observation is confirmed in fracture models with short-range elastic forces, which usually do not show scaling [10,11].

Most of the theoretical investigations in this field rely on large scale computer simulation of lattice models where the elastic medium is represented by a spring (beam) network, and disorder is captured either by random dilution or by assigning random failure thresholds to the bonds [12]. The failure rule usually applied in lattice models is discontinuous and irreversible: when the local load exceeds the failure threshold of a bond, the bond is removed from the calculations (*i.e.* its elastic modulus is set to 0). Furthermore, failed bonds are never restored (no healing). Very recently, a novel continuous damage law has been introduced in lattice models [13]. In the framework of this model when the failure threshold of a bond is exceeded the elastic modulus of the bond is reduced by a factor $a$ ($0 < a < 1$), furthermore, multiple failures of bonds are allowed. This description of damage in terms of a continuous parameter corresponds to consider the system at a length scale larger than the typical crack size. Computer simulations have revealed some remarkable features of the model: after some transients the system tends to a steady state which is macroscopically plastic, and is characterized by a power law distributed avalanches of breaking events.

A very important class of models of material failure are the fiber bundle models (FBM) [14–31], which have been extensively studied during the past years. These models consists of a set of parallel fibers having statistically distributed strength. The sample is loaded parallel to the fibers direction, and the fibers fail if the load on them exceeds their threshold value. In stress controlled experiments, after each fiber failure the load carried by the broken fiber is redistributed among the intact ones. Among the several theoretical approaches, one simplification that makes the problem analytically tractable is the assumption of global load transfer, which means that after each fiber breaking the stress is equally distributed on the intact fibers neglecting stress enhancement in the vicinity of failed regions [14–23,29–31]. The relevance of FBM is manifold: in spite of their simplicity these models capture the most important aspects of material damage and due

[a] e-mail: feri@dtp.atomki.hu

to the analytic solutions they provide a deeper understanding of the fracture process. Furthermore, they serve as a basis for more realistic damage models having also practical importance. The very successful micromechanical models of fiber reinforced composites are improved variants of FBM taking into account stress localization (local load transfer) [19–21,24], the effect of matrix material between fibers [20–23,29–31], and possible nonlinear behavior of fibers [16]. Previous studies of FBM addressed the macroscopic constitutive behavior, the reliability and size scaling of the global material strength, and the avalanches of fiber breaks preceding ultimate failure [10,11,32–36].

In this paper we generalize the FBM applying a continuous damage law for the elements in the spirit of reference [13]. Emphasis is put on the microstructure of damage and its evolution with increasing load. For the case of global load transfer in the continuous damage model, we derive an exact analytic expression for the constitutive behavior and show that the system reaches asymptotically a steady state, which is macroscopically plastic. It is demonstrated that the continuous damage model provides a broad spectrum of description of materials by varying its parameters and for special choices of the parameter values the model recovers the dry FBM and other micromechanical models of composites known in the literature. Next, we present a theoretical investigation of damaging in FBM by studying the 'dry' FBM varying the range of load transfer. In the case of global load transfer the model approaches the failure point by scaling laws, analogous to those observed close to a spinodal [8]. However, scaling is not observed for local load transfer FBM [10,11] as it is expected for a spinodal instability, which can only be observed in mean-field theory. Increasing the range of interactions, one can observe that the spinodal point, defined in the global load transfer FBM, is approached. The evolution of damage is compared in the local load transfer dry and continuous damage FBM. Finally, we analyze the effect of quenched random threshold on damage localization.

The paper is organized as follows: in Section 2 we describe the FBM and derive their constitutive behavior in Section 3. In Section 4 we discuss the local load transfer FMB focusing on the constitutive behaviour and on the cluster analysis, and in Section 5 we explore the role of the type of disorder in the evolution of damage. Section 6 is devoted to discussion and conclusions.

## 2 Models

The system under consideration is composed of $N$ fibers assembled in parallel on a two dimensional square lattice of side length $L$, *i.e.* $N = L^2$. The geometrical structure of the model is illustrated in Figure 1. The square lattice corresponds to a cross section of a unidirectional fiber ensemble. In FBM, the fibers are considered to be linearly elastic until breaking (brittle failure) with identical Young-modulus $E_f$ but with random failure thresholds $d_i$, $i = 1, \ldots, N$. The failure strength $d_i$ of individual fibers

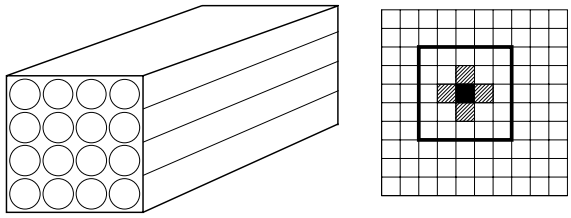

**Fig. 1.** The geometry of the FBM. The uniaxial fiber bundle (left) is modeled on a square lattice (right) corresponding to a cross section of the specimen. The black plaquette indicates a broken fiber, its nearest neighborhood is shadowed, and the bold line shows the neighborhood for the range of interaction $R = 2$.

is supposed to be independent identically distributed random variables with a cumulative probability distribution $P(d)$. The fiber bundle is supposed to be loaded uniaxially, and load $F$ applied parallel to the fibers gives rise to a strain $f$ of the bundle. When a fiber experiences a local load larger than its failure threshold the fiber fails. In dry FBM there is no matrix material present, which implies that broken fibers do not support load any more, and their load is redistributed to the surviving fibers.

In the global load transfer FBM, after failure the load is transfered equally to all the remaining intact fibers, so that the load on fiber $i$ is simply given by $F_i = F/n_{\rm s}(F)$, where $n_{\rm s}(F)$ is the total number of surviving fibers for a load $F$. This also implies that the range of interaction between fibers is infinite, and hence, the global load transfer corresponds to the mean field treatment of FBM. In the local load transfer FBM the load is transfered equally only to the surviving nearest neighbor fibers, giving rise to high stress concentration around failed regions (see also Fig. 1). We also study intermediate situations in which the load is transfered to a local neighborhood surrounding the failed fiber (*i.e.* a square of radius $R$ centered on the failed fiber, see Fig. 1). This model interpolates between the nearest neighbor local FBM and the global FBM as the range of interaction is increased.

Next we generalize the model replacing the brittle failure of fibers by a continuous damage parameter [13]. When the load on a fiber reaches the threshold value $d_i$ the stiffness $E_f$ of the fiber is reduced by a factor $0 < a < 1$. The characterization of damage by a continuous parameter corresponds to describe the system on length scales larger than the typical crack size. This can be interpreted such that the smallest elements of the model are fibers and the continuous damage is due to cracking inside fibers. However, the model can also be considered as the discretization of the system on length scales larger than the size of single fibers, so that one element of the model consists of a collection of fibers with matrix material in between. In this case the microscopic damage mechanism resulting in multiple failure of the elements is the gradual cracking of matrix and the breaking of fibers.

In the following the elements of the continuous damage FBM will be called fibers, but we have the above two possible interpretations in mind. Once the fiber $i$ has failed

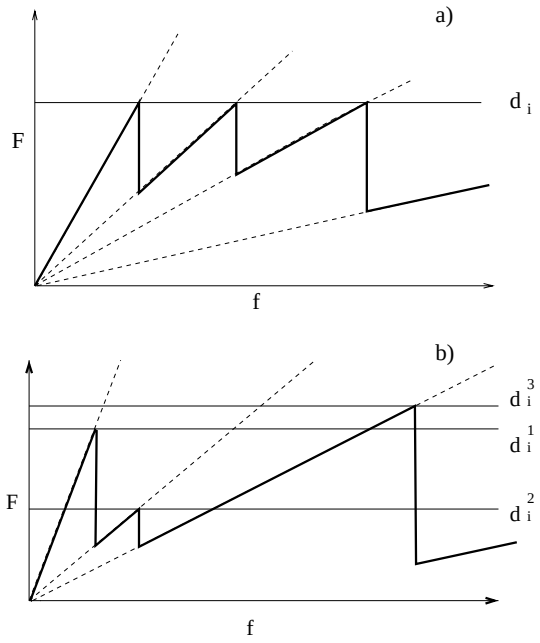


**Fig. 2.** The constitutive behavior of a single fiber of the continuous damage model when multiple failure is allowed. (a) Quenched disorder: the horizontal line indicates the damage threshold $d_i$, which is constant in time for each fiber. (b) Annealed disorder: a new threshold is extracted at random after each failure.

its load is reduced to $af_i$ and the rest of the load $(1-a)f_i$ is distributed equally among all the other fibers (global stress transfer) or among the neighboring fibers (local stress transfer). In principle, a fiber can now fail more than once and we define $k_{\max}$ as the maximum number of failures allowed per fiber. We will first study the model for finite $k_{\max}$ and eventually take the limit $k_{\max} \to \infty$. It is important to note that once a fiber has failed, we can either keep the same failure threshold (quenched disorder) or chose a different one of the same distribution (annealed disorder), which can model microscopic rearrangements in the material. The failure rules of the model in the two cases are illustrated in Figure 2. In the following sections we will analyze both cases, showing that there are differences in the microstructure of damage between quenched and annealed disorder in this problem.

## 3 Constitutive laws

Here we derive the constitutive law for continuous damage FBM and show how the FBMs used in the literature can be recovered in particular limits. We first consider the case in which fibers are allowed to fail only once: the constitutive equation reads as

$$\frac{F}{N} = f(1-P(f)) + afP(f), \tag{1}$$

where $P(f)$ and $1-P(f)$ are the fraction of failed and intact fibers, respectively, and the Young-modulus $E_f$ of intact fibers is taken to be unity. In equation (1) the first term provides the load carried by intact fibers while the second term is the contribution of the failed ones. Note that this particular case together with the parameter choice $a = 0$ (*i.e.* broken fibers carry no load) corresponds to the dry FBM [14,15,17,18], while setting $a = 0.5$ in equation (1) we recover the so-called micromechanical model of fiber reinforced ceramic matrix composites (CMC's), which has been extensively studied in the literature [25–28]. In CMC's the physical origin of the load bearing capacity of failed fibers is that in the vicinity of the broken face of the fiber the fiber-matrix interface debonds and the stress builds up again in the failed fiber through the sliding fiber-matrix interface.

When the fibers are allowed to fail more than once we have to distinguish between quenched and annealed disorder.

(i) *Quenched disorder*: When the fibers are allowed to fail twice the constitutive equation can be written as

$$\frac{F}{N} = f(1-P(f)) + af\left[P(f)-P(af)\right] + a^2 fP(af), \tag{2}$$

where $[P(f)-P(af)]$ is the fraction of those fibers which failed only once, and $P(af)$ provides the fraction of fibers which failed already twice. In the general case, when fibers are allowed to fail $k_{\max}$ times, where $k_{\max}$ can also go to infinity, the constitutive equation can be cast into the form

$$\frac{F}{N} = f(1-P(f)) + \sum_{i=1}^{k_{\max}-1} a^i f\left[P(a^{i-1}f) - P(a^i f)\right] + a^{k_{\max}} fP(a^{k_{\max}-1}f). \tag{3}$$

(ii) *Annealed disorder*: As in the previous case we consider first the case in which fibers are allowed to fail twice, obtaining

$$\frac{F}{N} = f(1-P(f)) + afP(f)(1-P(af)) + a^2 fP(f)P(af), \tag{4}$$

where $P(f)(1-P(af))$ is the fraction of fibers which failed only once, and $P(f)P(af)$ is the fraction of fibers which failed already twice. Finally, when fibers are allowed to fail $k_{\max}$ times, where $k_{\max}$ can also go to infinity, the constitutive equation is given by

$$\frac{F}{N} = \sum_{i=0}^{k_{\max}-1} a^i f\left[1-P(a^i f)\right] \prod_{j=0}^{i-1} P(a^j f) + a^{k_{\max}} f \prod_{i=0}^{k_{\max}-1} P(a^i f). \tag{5}$$

In Figure 3 we show the explicit form of the constitutive law for quenched disorder for different values of $k_{\max}$ in the case of the Weibull distribution

$$P(d) = 1 - \exp(-(d/d_c)^m), \tag{6}$$

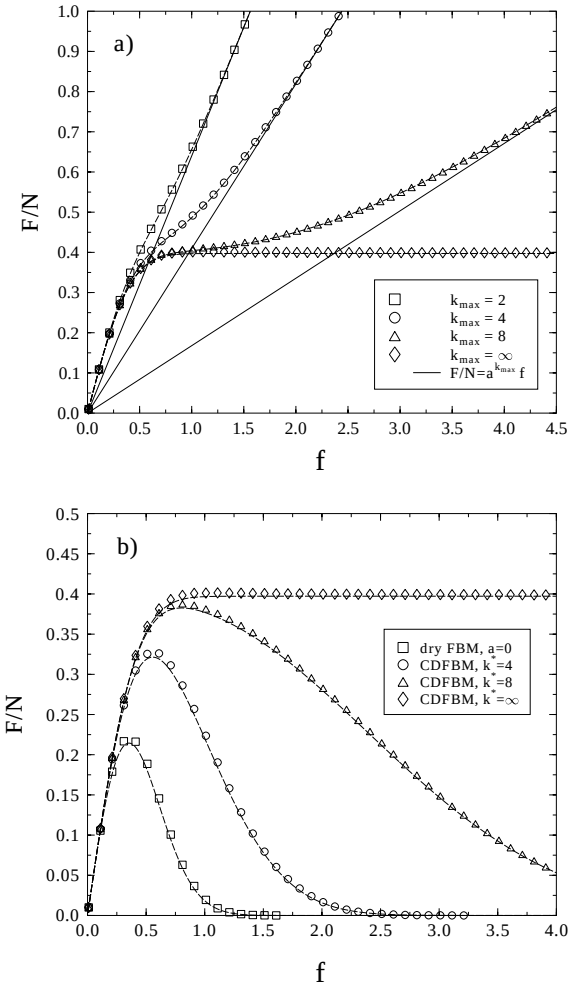


**Fig. 3.** (a) The constitutive law for the global stress transfer continuous damage FBM (CDFBM) for different values of $k_{\max}$ for $m = 2.0$, $a = 0.8$ and quenched disorder. Plastic behavior is obtained in the limit of $k_{\max} \to \infty$. (b) Comparison between dry and continuous damage FBM. If we allow for brittle failure after $k^*$ damage events, we obtain a plastic plateau followed by brittle failure. Symbols refer to simulations of bundles of size $N = 128^2$ and lines to the analytic calculations.

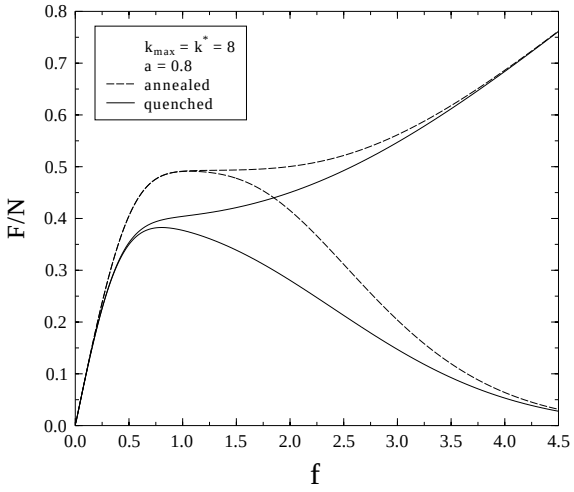


**Fig. 4.** Comparison of the constitutive laws of the quenched and annealed case for $a = 0.8$, $k_{\max} = 8$ and $k^* = 8$.

where $m$ is the Weibull modulus and $d_c$ denotes the characteristic strength of fibers. It is important to remark that the constitutive laws derived above are exact only in the infinite size limit ($N \to \infty$), while fluctuations in the value of the failure stress $F_c$ have been observed and studied for finite size bundles. For this reason, we compare the theoretical results with numerical simulations of bundles of size $N = 128^2$. The agreement between simulations and theory turns out to be satisfactory both for quenched (Fig. 3) and annealed disorder and reflects the fact that for global load sharing finite size fluctuations, for instance for $F_c$, should scale as $1/\sqrt{(N)}$. This behavior has to be contrasted with local-load sharing fiber bundles where finite size effects are very strong, as we will discuss in the following.

In Figure 3a the fibers are supposed to have $a^{k_{\max}}$ residual stiffness after having failed $k_{\max}$ times, which gives rise to hardening of the material, *i.e.* the $F/N$ curves asymptotically tend to straight lines with slope $a^{k_{\max}}$. Increasing $k_{\max}$ the hardening part of the constitutive behavior is preceded by a longer and longer plastic plateau, and in the limiting case of $k_{\max} \to \infty$ the materials behavior becomes completely plastic (see Fig. 3). A similar plateau and asymptotic linear behavior has been observed in brittle matrix composites, where the multiple cracking of matrix turned to be responsible for the relatively broad plateau of the constitutive behavior, and the asymptotic linear part is due to the linear elastic behavior of fibers remained intact after matrix cracking [40].

In order to describe macroscopic cracking and global failure instead of hardening, the residual stiffness of the fibers has to be set to zero after a maximum number $k^*$ of allowed failures [13]. In this case the constitutive law can be obtained from the general form equations (3, 5) by skipping the last term corresponding to the residual stiffness of fibers, and by setting $k_{\max} = k^*$ in the remaining part. A comparison of the constitutive laws of the dry and continuous damage FBM is presented in Figure 3b for the case of quenched disorder. Annealed disorder yields similar results. One can observe that the dry FBM constitutive law has a relatively sharp maximum, however, the continuous damage FBM curves exhibit a plateau whose length increases with increasing $k^*$. Note that the maximum value of $F/N$ corresponds to the macroscopic strength of the material and in stress controlled experiments the plateau and the decreasing part of the curves cannot be reached. However, by controlling the strain $f$, the plateau and the decreasing regime can also be realized. The value of the driving stress $\sigma \equiv F/N$ corresponding to the plastic plateau is determined by the damage parameter $a$, while the length of the plateau is controlled by $k_{\max}$ and $k^*$.

In Figure 4, we directly compare the constitutive law for quenched and annealed disorder and confirm that the differences between the cases are very small. In particular,

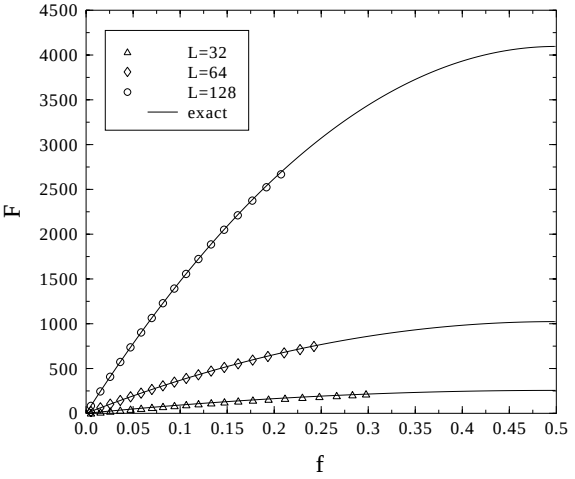


**Fig. 5.** The constitutive law for the global stress transfer dry FBM (solid line) is compared with the local stress transfer model. Increasing the system size the failure stress decreases.

all the basic constitutive behavior are reproduced in the two cases.

It is important to remark that the behavior of the dry FBM model ($a = 0$) under unloading and reloading to the original stress level is completely linear, since no new damage can occur during unloading-reloading sequences and the effect of the matrix material is completely neglected. This also implies that in each damage state the model is completely characterized by the Young modulus defined as the slope of the unloading curve. If the value of the damage parameter is larger than 0 ($a > 0$) the behavior of the system under unloading and reloading is rather complicated. Due to the sliding of broken fibers with respect to the matrix, hysteresis loops and remaining inelastic strain occur (for examples see Ref. [38] and references therein).

## 4 Local load transfer FBM

### 4.1 Constitutive behaviour

To study the effect of stress enhancement around failed fibers on the damage evolution and on the macroscopic constitutive behavior we employ local load transfer for the stress redistribution after fiber failure [20,25–27]. Since this case cannot be treated analytically, we perform numerical simulations in the dry FBM model: after fiber failure the load is redistributed on the intact nearest neighbors of the failed fiber using periodic boundary condition on the square lattice (see also Fig. 1). For simplicity, in this case the strength of fibers $d_i$ has a uniform distribution between 0 and 1. The algorithm to simulate the loading process is as follows: (i) we impose on all the fibers the same load, equal to the smallest failure threshold, which results in breaking of the weakest element. (ii) The load carried by the failed fiber is redistributed on the intact nearest neighbors, and the load of the broken fiber is set to zero. (iii) After the stress redistribution, those fibers whose load exceeds their failure threshold $d_i$ are identified and removed from the calculation, and the simulation is continued with point (ii). If the configuration obtained after the stress redistribution is stable, the global load is increased to cause the failure of one more fiber and the simulation is continued with point (ii). This procedure goes on until all fibers are broken. The applied stress just before global failure is considered to be the failure strength of the model solid. Simulations were performed with system sizes $L = 16, 32, 64, 128$.

The constitutive behavior of the local and global load transfer dry FBM is compared in Figure 5. For clarity, the total force $F$ (instead of stress) is presented as a function of strain $f$, for several different system sizes $L$. Note that $N = L^2$ is chosen the same for global and local load sharing simulations. In the case of global load transfer the $N \to \infty$ constitutive law can be obtained exactly by substituting the cumulative probability distribution $P(f) = f$ of the uniform distribution into the general form equation (1) and setting the damage parameter $a = 0$:

$$F = Nf(1 - P(f)) = Nf(1 - f), \qquad f \in [0, 0.5], \quad (7)$$

the strain corresponding to macroscopic failure is $f_c = 0.5$. It can be seen in Figure 5 that the macroscopic constitutive behavior for local load transfer always coincides with the global FBM solution, however, the macroscopic failure strength is substantially reduced in the local case giving rise to more brittle constitutive behavior. It is interesting to note that increasing the system size $L$ the failure strength of the local FBM decreases, showing the logarithmic size effect also found in the one-dimensional local FBM [11] and in two-dimensional fuse networks [37], while the global load transfer case does not have size dependence.

To get a deeper understanding of the behavior of the system as a function of the range $R$ of load redistribution, we perform simulations by redistributing the load after fiber failure on the intact fibers in a square of side length $2R + 1$ centered on the failed fiber. The range of load redistribution $R$ is varied between 1 and $(L - 1)/2$. Note that $R = 1$ corresponds to local load transfer on nearest and next-nearest neighbors, while the limiting case of $R = (L - 1)/2$ recovers the 'infinite' range global load transfer. The comparison of the constitutive behavior in the local and global load transfer case is presented in Figure 6. Simulations reveal that the constitutive laws obtained at different $R$ values always fall onto the curve of the global load transfer case and the macroscopic failure strength increases with increasing range of interaction $R$ approaching the strength of global FBM. For clarity, in Figure 6 we indicated by vertical dashed lines the position of global failure at different values of $R$.

To characterize the elastic response of the dry FBM model in a given damage state, we compute the Young modulus $Y$, defined as the slope of unloading curves as a function of the driving stress $\sigma \equiv F/N$:

$$Y(\sigma) = \frac{\sigma}{f(\sigma)} = 1 - P(f(\sigma)) = 1 - f(\sigma). \qquad (8)$$

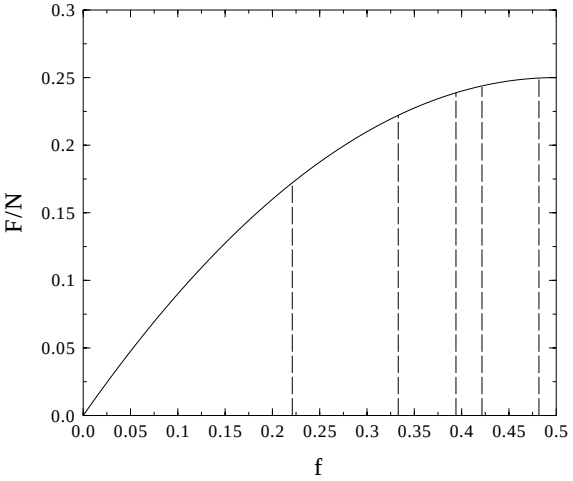


**Fig. 6.** The constitutive law for the global stress transfer dry FBM (solid line) is compared with the local stress transfer FBM for different interaction ranges $R$. The values of $R$ corresponding to the consecutive vertical dashed lines are $1, 3, 5, 11, 15$ from left to right, and the system size $L = 128$ was chosen. Increasing the interaction range the failure stress increases approaching the value predicted by the global stress transfer model.

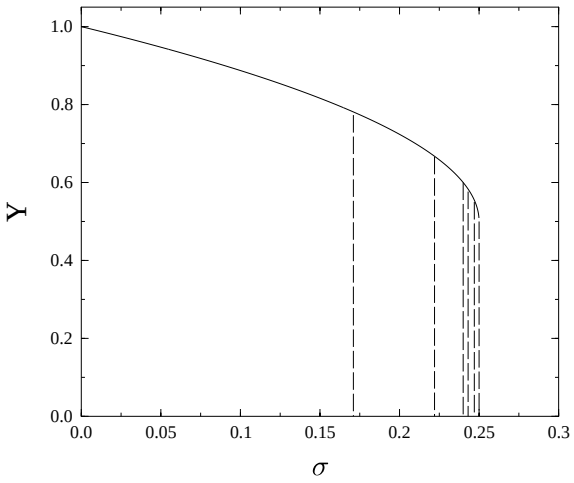


**Fig. 7.** The Young modulus for the global stress transfer dry FBM is compared with the local stress transfer model for different interaction ranges $R$. The values of $R$ corresponding to the vertical dashed lines are the same as in Figure 6.

Using the constitutive law (7) for the global load transfer case, $Y$ can be written into a closed form as a function of stress

$$Y(\sigma) = \frac{1}{2}\left[1 + \sqrt{1 - 4\sigma}\right]. \tag{9}$$

The results on $Y$ for global and local load transfer are shown in Figure 7, where the vertical dashed lines indicate the position of macroscopic failure at different values of the redistribution range $R$. It can be seen that at the failure point $Y(\sigma)$ has a discrete jump, the size of which decreases with increasing $R$, but it remains finite in the limit of global load transfer. Increasing $R$ gives rise to increasing slope of $Y(\sigma)$ at the failure point, and in the limit of infinite range interaction the tangent of $Y(\sigma)$ becomes vertical at the point of failure.

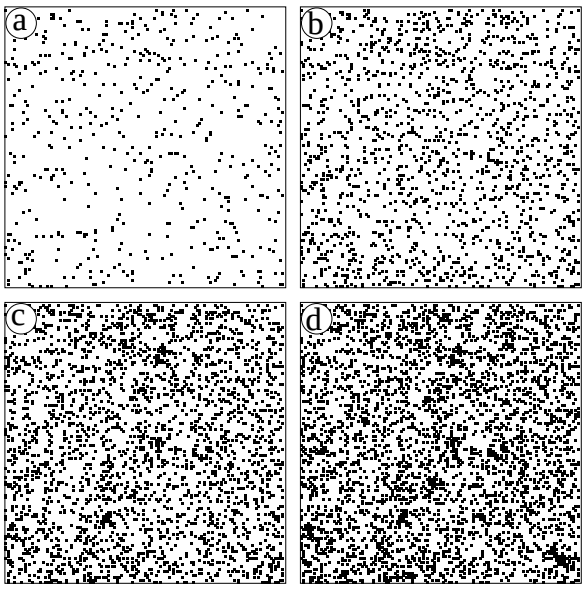


**Fig. 8.** Snapshots of the damage in the dry FBM model on a square lattice of size $L = 128$ for different values of the load: a) $F/F_c = 0.153$ b) $F/F_c = 0.468$, c) $F/F_c = 0.796$, d) $F/F_c = 0.997$.

### 4.2 Cluster analysis

One of the most interesting aspects of the damage mechanism of disordered solids is that the breakdown is preceded by an intensive precursor activity in the form of avalanches of microscopic breaking events. Under a given external load $F$ a certain fraction of fibers fails immediately. Due to the load transfer from broken to intact fibers this primary fiber breaking may initiate secondary breaking that may also trigger a whole avalanche of breaking. If $F$ is large enough the avalanche does not stop and the material fails catastrophically. It has been shown by analytic means that in the case of global load transfer the size distribution of avalanches follows asymptotically a universal power law with an exponent $-5/2$ [11,32], however, in the case of local load transfer no universal behavior exists, and the avalanche characteristic size is bounded [10,11]. This precursory activity can also be observed experimentally by means of the acoustic emission analysis. Acoustic emission measurements have revealed that for a broad variety of disordered materials the response to an increasing external load takes place in bursts having power law size distribution over a wide range [5–7].

In this section we analyze the evolution of damage in local load transfer FBM, comparing dry and continuous damage models. Instead of avalanches of fiber failures, we

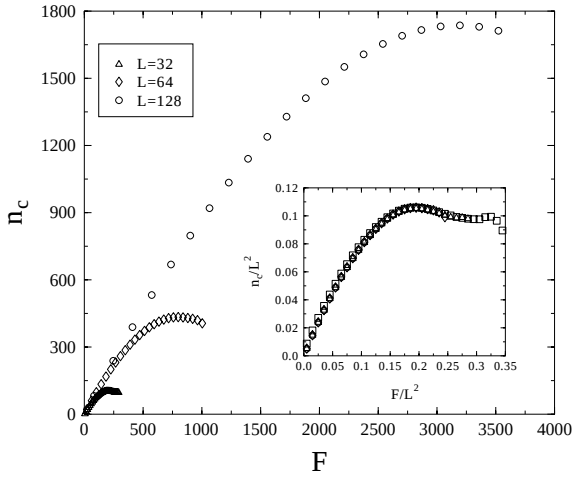


**Fig. 9.** The number of clusters as a function of the load $F$ in the local stress transfer dry FBM for different system sizes. In the inset the rescaled plot is presented, where also the system $L = 16$ is shown (square).

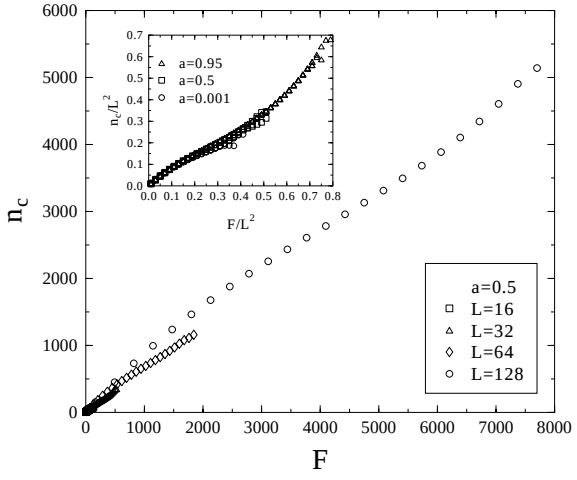


**Fig. 10.** The number of clusters as a function of the load $F$ in the local stress transfer continuous damage annealed FBM for different system sizes at $a = 0.5$. In the inset we show the rescaled plot for different values of $a$ and $L$.

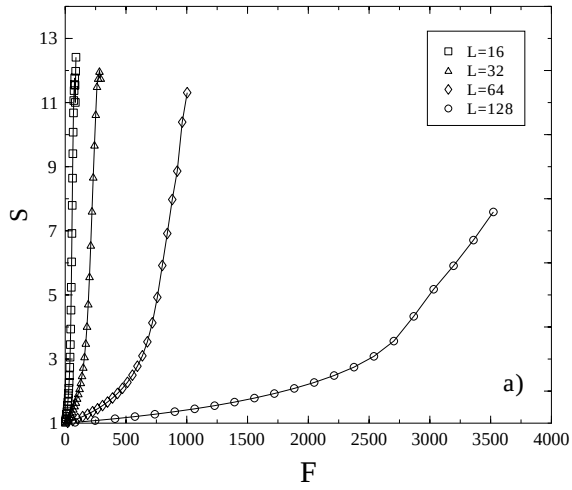


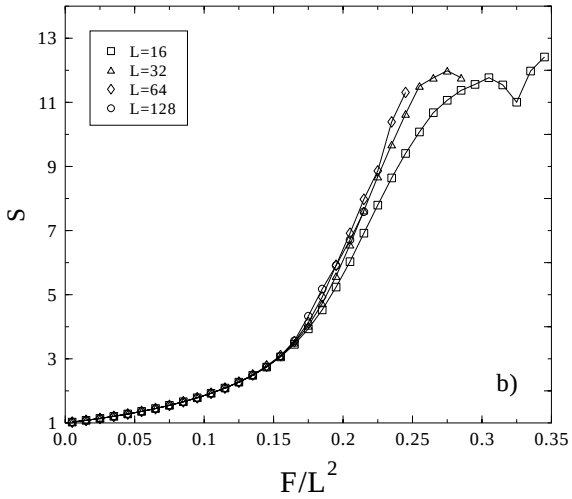


**Fig. 11.** (a) The average cluster size as a function of the load $F$ in the local stress transfer dry FBM for different system sizes $L$ and the corresponding rescaled plot (b).

focus on the properties of clusters of broken fibers which are much less explored. In the following simulations we employ a uniform distribution for the thresholds $d_i$. The load after fiber failure is redistributed on the surviving nearest neighbors. As the load is increased, fiber breaks and clusters of broken fibers are formed due to the spatial correlation introduced by the local load transfer. These clusters of broken fibers can be identified as microcracks formed in the plane perpendicular to the load direction. We monitor the damage evolution by taking snapshots of the clusters at different loads. In Figure 8 the damage evolution is shown in the dry FBM. One can observe the nucleation and gradual growth of clusters with increasing load $F$. We find that the clusters are small compared to the system size even before global failure (see Fig. 8d), in accordance with the first-order transition scenario. In the continuous damage FBM with local load transfer the clusters of failed fibers are defined as connected sets of fibers having the same number of failure, taking into account only nearest neighbor connections. In these calculations we set $k_{\max} = \infty$, and the simulations are stopped when the plastic regime is reached.

To obtain quantitative informations on the damage evolution, we measure the cluster probability distribution $n(s, F)$, defined as the number of clusters formed by $s$ neighboring broken fibers when the applied load is $F$ [8]. The moments ($M_k(F) \equiv \int s^k n(s, F) \mathrm{d}s$ is the $k$th moment) of $n(s, F)$ contain most of the information on the evolution of the damage. We determine $n(s, F)$ for different system sizes $L$ by averaging over the disorder. The total number of clusters $n_c \equiv M_0$ as a function of the load is presented in Figure 9. The increasing part of $n_c$ as a function of $F$ is due to the nucleation of new microcracks, and the short plateau or decreasing regime

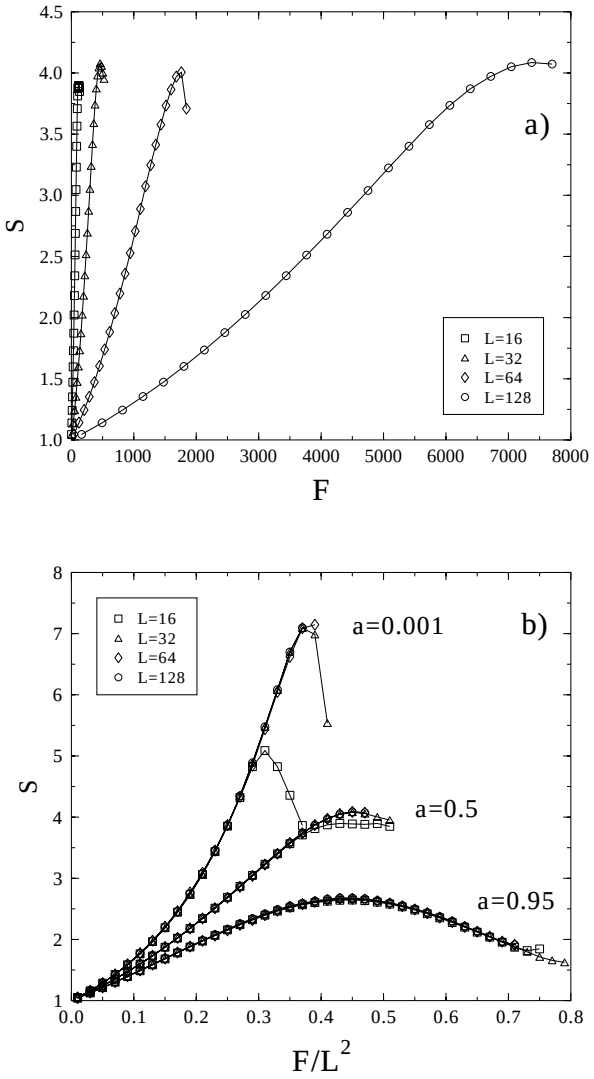


**Fig. 12.** (a) The average cluster size as a function of the load $F$ in the local stress transfer continuous damage annealed FBM with $a = 0.5$ for different system sizes $L$, and (b) the corresponding rescaled plot for different values of $L$ and $a$.

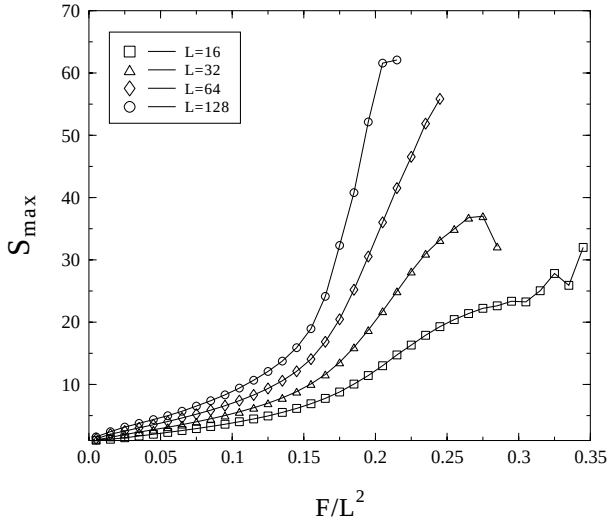


**Fig. 13.** The size of the largest cluster $S_{\max}$ as a function of $F/L^2$ in the local stress transfer dry FBM for different system sizes $L$.

in the vicinity of global failure is caused by the coalescence of growing cracks. The inset of Figure 9 demonstrates that in dry FBM $n_c$ obeys a simple scaling law $n_c = L^2 g(F/L^2)$ implying that the clusters are homogeneously scattered through the lattice. A similar scaling is observed for the continuous damage annealed FBM in Figure 10. The inset shows that the scaling function is independent of the damage parameter $a$.

Next, we measure the average cluster size defined as $S \equiv M_2/M_1$ and show that it approaches a value which decreases with system size (Fig. 11a). It can be seen that for a given system size the $S(F)$ curves have two regimes: a slowly increasing initial regime due to the nucleation and growth of clusters, and a rapidly increasing part close to global failure which is caused by the coalescence of growing cracks. In dry FBM, we can simply rescale the data according to the law $S(F, L) = s(F/L^2)$ and obtain a good collapse (Fig. 11b). Similar results are obtained for the continuous damage case, but we see that the rescaled curves depend on $a$ (Fig. 12). The larger $a$ is, the smaller the clusters are, since the stress concentration decreases with increasing $a$, and the disorder gets more dominating. These results demonstrate that global failure is initiated once the crack size reaches a critical size $s_c$ after which a crack becomes unstable. However, the average cluster size $S$ does not provide a reliable estimate of $s_c$, which can be obtained instead monitoring the size of the largest cluster $S_{\max}$ as a function of the load. It can be seen in Figure 13 that $S_{\max}$ reaches a value that increases with $L$, but for large $L$ this value seems to saturate. The rapid increase of $S_{\max}$ close to the failure point is due to the coalescence of clusters and is thus produced by a very small amount of fiber failures.

## 5 Damage localization: effect of the quenched disorder

In the previous section, we analyzed the damage structure in the local load transfer models. In the dry FBM and in the case of continuous damage FBM with annealed disorder we do not expect to find any non trivial damage localization for global load transfer rules, since these models behave effectively like in mean-field theory. On the other hand, quenched disorder can lead to localized structure for continuous damage FBM even in global load transfer conditions. Weak fibers are expected to fail more times generating an inhomogeneous damage pattern.

In order to analyze this effect, we measure $k(i)$, the number of failures at fiber $i$, when there is exactly one fiber, which has reached $k_{\max}$. In the bottom part of Figure 14 we plot the value of $k(i)$ and the corresponding

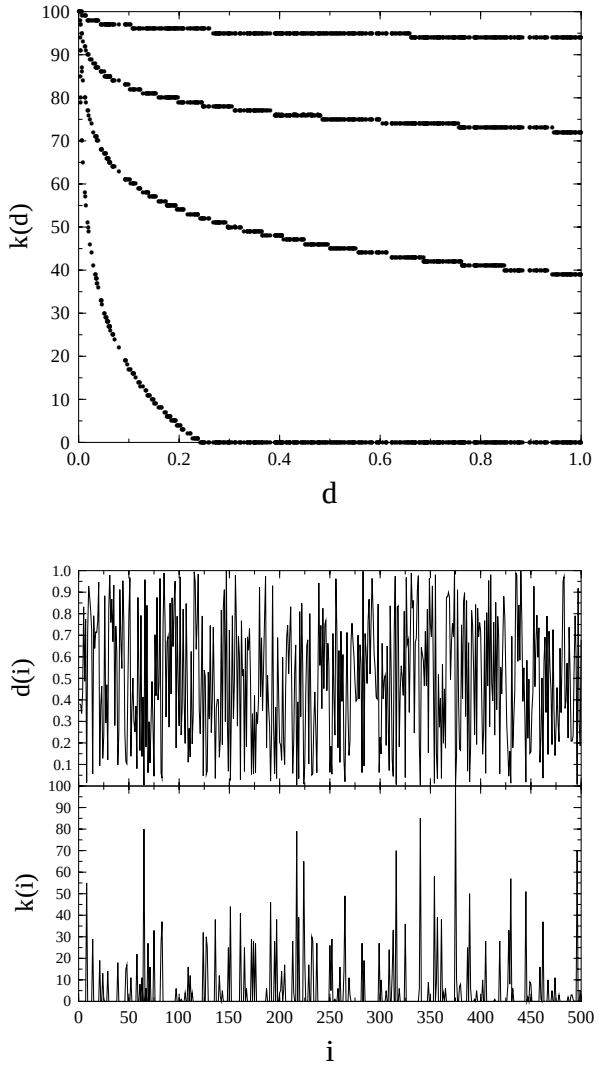


**Fig. 14.** The number of failures $k$ of the fibers as a function of their threshold $d$ (distributed uniformly) in the quenched global load transfer continuous FBM (top). The parameters used are $k_{\max} = 100$, $N = 500$ and $a = 0.4, 0.8, 0.9, 0.95$. The threshold $d(i)$ as a function of $i$ is compared with the 'damage' $k(i)$ for $a = 0.9$ (bottom).

value of the threshold $d(i)$. The 'damage' $k(i)$ shows a very irregular pattern, which should be compared with a roughly uniform structure expected for annealed disorder. In the upper part of the figure we display the decay of $k$ as a function of $d$, showing how weak fibers break more often than strong ones. The decay is more pronounced when $a$ is close to one, and becomes less important for smaller $a$. It is straightforward to obtain an analytic expression for $k(d)$ which is compared with the numerical results in Figure 15.

Finally, we expect that quenched disorder should have an effect also on the cluster structure of local load transfer models. In order to confirm this point, we compare the number of clusters $n_c(F)$ and the average cluster size $S$ for quenched and annealed disorder. The results, shown in

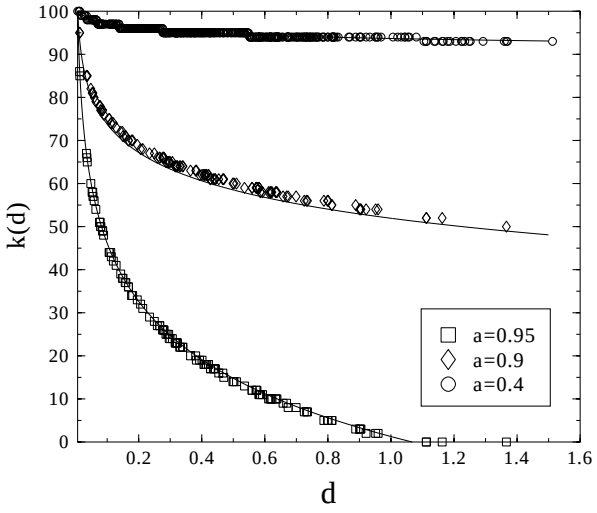


**Fig. 15.** The number of failures $k$ of the fibers as a function of their threshold $d$ (distributed according to the Weibull distribution with $m = 1.5$) in the quenched global load transfer continuous FBM: comparison between simulations and analytic results for $a = 0.95, 0.9, 0.4$.

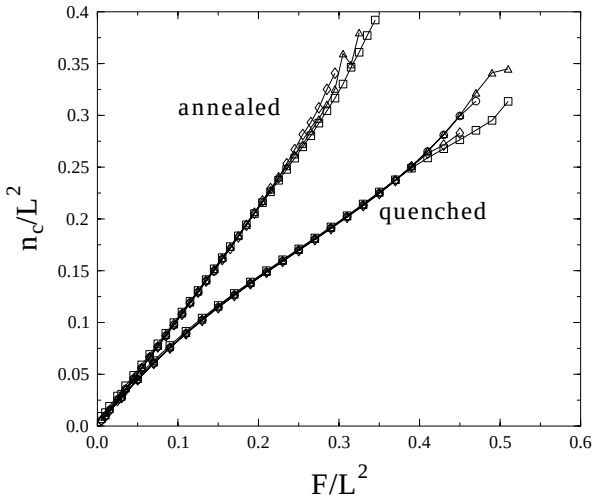


**Fig. 16.** The number of clusters as a function of the rescaled load $F/L^2$ in the local stress transfer continuous damage quenched and annealed FBM for different system sizes at $a = 0.5$. Note that the number of clusters increases faster for annealed disorder indicating a smaller degree localization.

Figures 16 and 17, indicate that damage is more localized when the disorder is quenched.

## 6 Conclusions

We have proposed a continuous damage version of the FBM, that can be used to model a wide variety of constitutive behaviors. We have analyzed the development of damage in FBM under different conditions and compared the local load transfer model with different interaction

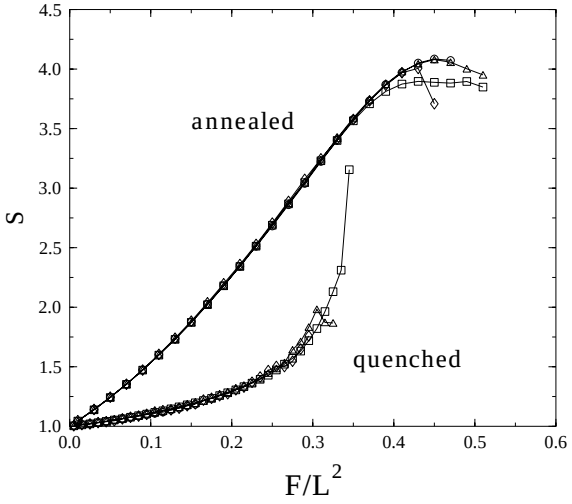


**Fig. 17.** The average cluster size as a function of the rescaled load $F/L^2$ in the local stress transfer continuous damage quenched and annealed FBM for different system sizes at $a = 0.5$. Note that the cluster size increases faster for quenched disorder indicating a larger degree localization.

ranges with the global load transfer model that can be solved exactly in the limit $N \to \infty$.

From the theoretical point of view, the cluster analysis shows the analogies between the failure in the FBM and nucleation in first-order phase transition. The failure point in global load transfer FBM plays the role of a spinodal point. The strain $f$ carried by the fibers, proportional to the fraction of intact fibers [8], close to the failure load $F_c$ has a diverging derivative $df/dF \sim (F_c - F)^{-1/2}$. A similar behavior is observed close to a spinodal instability in first-order phase transitions. One should note that the spinodal point and its associated scaling is a mean-field property, obtained in the limit $N \to \infty$, and in general is not observed for finite dimensional short-ranged models where nucleation occurs much before reaching the spinodal. Similarly, in local-load transfer (*i.e.* short range) FBM failure occurs much before the corresponding global load sharing instability (*i.e.* the spinodal) and the avalanche characteristic size is bounded [10,11,32].

We have shown that increasing the range of interaction the failure point is shifted towards the spinodal. A similar behavior is observed for instance in Ising systems when the range of interactions is increased [39]. In models with long range stress transfer, as for instance in elastic or electric networks, it is possible to observe the spinodal scaling even in finite dimensional systems [8,11]. The presence of a spinodal instability could explain the observation of scaling properties in acoustic emission experiments [5–7].

Our continuous damage FBM can reproduce a wide variety of elasto-plastic constitutive behaviors. A remarkable feature of the model is that multiple failure of the elements results in ductile macroscopic behavior in spite of the brittleness of the constituents. Similar ductile behavior has been observed experimentally in fiber reinforced composites made of brittle constituents [42–44]. Experiments revealed that the mechanism of this ductility, which is called pseudo-strain hardening, is the multiple failure of the material [42–44]. Our continuous damage model, recovering as special cases the dry bundle model and micromechanical models known in the literature, could provide a general framework for the statistical-micromechanical modeling of the behavior of fiber reinforced composites. The fitting of experimental results in the framework of our model will be presented in a forthcoming publication.

This work was supported by the project SFB381. F.K. acknowledges financial support from the Alexander von Humboldt Foundation (Roman Herzog Fellowship). F.K. is grateful to I. Sajtos for the valuable discussions. S.Z. acknowledges financial support from EC TMR Research Network under contract ERBFMRXCT960062.

## References

1. A. Buchel, J.P. Sethna, Phys. Rev. Lett. **77**, 1520 (1996); Phys. Rev. E **55**, 7669 (1997).
2. J.B. Rundle, W. Klein Phys. Rev. Lett. **63**, 171 (1989).
3. R.L.B. Selinger, Z.-G. Wang, W.M. Gelbart, A. Ben-Saul, Phys. Rev. A **43**, 4396 (1991); Z.-G. Wang, U. Landman, R.L.B. Selinger, W.M. Gelbart, Phys. Rev. B **44** 378 (1991).
4. R.L.B. Selinger, Z.-G. Wang, W.M. Gelbart, J. Chem. Phys. **95**, 9128 (1991).
5. A. Garcimartín, A. Guarino, L. Bellon, S. Ciliberto, Phys. Rev. Lett. **79**, 3202 (1997); A. Guarino, A. Garcimartín, S. Ciliberto, Eur. Phys. J. B **6**, 13 (1998).
6. C. Maes, A. van Moffaert, H. Frederix, H. Strauven, Phys. Rev. B **57**, 4987 (1998).
7. A. Petri, G. Paparo, A. Vespignani, A. Alippi, M. Costantini, Phys. Rev. Lett. **73**, 3423 (1994).
8. S. Zapperi, P. Ray, H.E. Stanley, A. Vespignani, Phys. Rev. Lett. **78**, 1408 (1997); Phys. Rev. E **59**, 5049 (1999).
9. C. Unger, W. Klein, Phys. Rev. B **29**, 2698 (1984); *ibidem* **31**, 6127 (1985). For a review on spinodal nucleation see L. Monette, Int. J. Mod. Phys B **8**, 1417 (1994).
10. M. Kloster, A. Hansen, P.C. Hemmer, Phys. Rev. E **56**, 2615 (1997).
11. A. Hansen, P.C. Hemmer, Phys. Lett. A **184**, 394 (1994).
12. *Statistical models for the fracture of disordered media*, edited by H.J. Herrmann, S. Roux (North-Holland, Amsterdam, 1990).
13. S. Zapperi, A. Vespignani, H.E. Stanley, Nature (London) **388**, 658 (1997).
14. H.E. Daniels, Proc. R. Soc. London **A 183**, 405 (1945).
15. B.D. Coleman, J. Appl. Phys. **29**, 968 (1958).
16. D. Krajcinovic, M.A.G. Silva, Int. J. Solids Struct. **18**, 551 (1982).
17. D. Sornette, J. Phys. A **22**, L243 (1989).
18. D. Sornette, J. Phys. France **50**, 745 (1989).
19. C. Moukarzel, P.M. Duxbury, J. Appl. Phys. **76**, 1 (1994).
20. D.G. Harlow, S.L. Phoenix, J. Composite Mater. **12**, 195 (1978).

21. R.L. Smith, S.L. Phoenix, J. Appl. Mech. **48**, 75 (1981); D.G. Harlow, S.L. Phoenix, J. Mech. Phys. Solids **39**, 173 (1991).
22. S.L. Phoenix, M. Ibnabdeljalil, C.-Y. Hui, Int. J. Solids Struct. **34**, 545 (1997).
23. S.L. Phoenix, Raj, Acta Metall. Mater. **40**, 2813 (1992).
24. I.J. Beyerlein, S.L. Phoenix, J. Mech. Phys. Solids **44**, 1997 (1996).
25. W.A. Curtin, J. Am. Ceram. Soc. **74**, 2837 (1991).
26. W.A. Curtin, J. Mech. Phys. Solids **41**, 217 (1993).
27. S.J. Zhou, W.A. Curtin, Acta. Metal. Mater. **43**, 3093 (1995).
28. F. Hild, A. Burr, F.A. Leckie, Eur. J. Mech. A **13**, 731 (1994).
29. W.A. Curtin, N. Takeda, J. Comp. Matls. **32**, 2042 (1998).
30. W.A. Curtin, J. Am. Ceram. Soc. **74**, 2837 (1991).
31. W.A. Curtin, Phys. Rev. Lett. **80**, 1445 (1998).
32. P.C. Hemmer, A. Hansen, J. Appl. Mech. **59**, 909 (1992).
33. W.I. Newman, A.M. Gabrielov, T.A. Durand, S.L. Phoenix, D.L. Turcotte, Physica D **77**, 200 (1994).
34. W.I. Newman, D.L. Turcotte, A.M. Gabrielov, Phys. Rev. E **52**, 4827 (1995).
35. Y. Moreno, J.B. Gomez, A.F. Pacheco, Physica A **274**, 400 (1999).
36. R. da Silveira, Phys. Rev. Lett. **80**, 3157 (1998).
37. P. Duxbury, P.D. Beale, P.L. Leath, Phys. Rev. Lett. **57**, 1052 (1986).
38. F. Kun, H.J. Herrmann, appearing in J. Mater. Sci.
39. D. Heerman, W. Klein, D. Stauffer, Phys. Rev. Lett. **49** 1262 (1982); T. Ray, W. Klein, J. Stat. Phys. **61**, 891 (1990).
40. A.G. Evans, F.W. Zok, J. Mater. Sci. **29**, 3857 (1994).
41. S.M. Spearing, F.W. Zok, J. Eng. Mater. Technol. **115**, 314 (1993).
42. A.E. Naaman, H.W. Reinhardt, *High performance fiber reinforced cement composites* (E & FN Spon, London, 1995).
43. A.G. Evans, J.M. Domergue, E. Vagaggini, J. Am. Ceramic Soc. **77**, 1425 (1994).
44. T. Kanada, V.C. Li, J. Eng. Mech. **125**, 290 (1999).